The FASEB Journal
The Journal of the Federation of American Societies for Experimental Biology
All Articles | Submit | Subscribe | What's New | RSS

FASEB J. 2019 Jun; 33(6): 7778–7790. Published online 2019 Mar 20. doi: 10.1096/fj.201802799R: 10.1096/fj.201802799R

PMCID: PMC6529344 | PMID: 30894018

PDK4 drives metabolic alterations and muscle atrophy in cancer cachexia

Fabrizio Pin,[*†] Leah J. Novinger,[‡] Joshua R. Huot,[†§] Robert A. Harris,[¶] Marion E. Couch,[†‡‖#] Thomas M. O'Connell,[†‡‖#] and Andrea Bonetto[*†‡§‖#,1]

[*]Department of Anatomy and Cell Biology, Indiana University School of Medicine, Indianapolis, Indiana, USA;
[†]Indiana University–Purdue University Indianapolis Center for Cachexia Research, Innovation, and Therapy, Indiana University School of Medicine, Indianapolis, Indiana, USA;
[‡]Department of Otolaryngology–Head and Neck Surgery, Indiana University School of Medicine, Indianapolis, Indiana, USA;
[§]Department of Surgery, Indiana University School of Medicine, Indianapolis, Indiana, USA;
[¶]Department of Biochemistry and Molecular Biology, Indiana University School of Medicine, Indianapolis, Indiana, USA;
[‖]Simon Cancer Center, Indiana University School of Medicine, Indianapolis, Indiana, USA;
[#]Indiana Center for Musculoskeletal Health, Indiana University School of Medicine, Indianapolis, Indiana, USA
[1]Correspondence: Department of Surgery, Indiana University School of Medicine, 980 W Walnut St., R3-C522, Indianapolis, IN 46202, USA., E-mail: abonetto@iu.edu

Received 2018 Dec 22; Accepted 2019 Mar 4.

Abstract

Cachexia is frequently accompanied by severe metabolic derangements, although the mechanisms responsible for this debilitating condition remain unclear. Pyruvate dehydrogenase kinase (PDK)4, a critical regulator of cellular energ

was found elevated in experimental models of cancer, starvation, diabetes, and sepsis. Here we aimed to investigate the link between PDK4 and the changes in muscle size in cancer cachexia. High PDK4 and abnormal energetic metabolism were found in the skeletal muscle of colon-26 tumor hosts, as well as in mice fed a diet enriched in Pirinixic acid, previously shown to increase PDK4 levels. Viral-mediated PDK4 overexpression in myotube cultures was sufficient to promote myofiber shrinkage, consistent with enhanced protein catabolism and mitochondrial abnormalities. On the contrary, blockade of PDK4 was sufficient to restore myotube size in C2C12 cultures exposed to tumor media. Our data support, for the first time, a direct role for PDK4 in promoting cancer-associated muscle metabolic alterations and skeletal muscle atrophy.—Pin, F., Novinger, L. J., Huot, J. R., Harris, R. A., Couch, M. E., O'Connell, T. M., Bonetto, A. PDK4 drives metabolic alterations and muscle atrophy in cancer cachexia.

Keywords: skeletal muscle atrophy, energy metabolism, chemotherapy, mitochondria, C2C12 myotubes

---

A majority of cancer patients experience symptoms of cachexia. Such a condition is mainly characterized by dramatic weight loss, including adipose tissue and skeletal muscle, as well as a reduced response to anticancer treatments and poorer survival (1, 2). No treatments have been approved for the management of cachexia, and it is estimated that such a disorder directly accounts for over 20% of cancer deaths (3). The clinical presentation of cachexia is heterogeneous. Along with dramatic skeletal muscle depletion, cachexia involves profound systemic derangements, including abnormal initiation of protein breakdown, dyslipidemia, elevated inflammatory response, altered activation of muscle-specific signaling pathways, induction of apoptosis, and muscle mitochondrial dysfunctions (2, 4–7). Consequently, the loss of skeletal muscle associated with cancer development is also frequently accompanied by a multitude of metabolic disturbances. Using comprehensive metabolomic profiling, we recently showed that cancer-induced cachexia is characterized by a number of unique metabolic derangements. These include up-regulated systemic glucose demand, significant depletion of liver glucose and glycogen, and dramatically increased levels of LDL particles. In addition to these changes is a distinct reduction in pyruvate dehydrogenase (PDH) and succinate dehydrogenase (SDH) enzymatic activities, as well as decreased overall muscle energy metabolite levels, including ATP and creatine phosphate, in the skeletal muscle of tumor hosts (8).

Interestingly, skeletal muscle exhibits a remarkable metabolic flexibility in fuel usage in response to various metabolic challenges, including energy deprivation, changes in food intake, and exercise (9–11). For example, during contraction, skeletal muscle utilizes blood glucose and stored glycogen as its first energy source, although in the case of prolonged exercise, an increasing fraction of the required energy is derived from fat oxidation. In a similar manner, fasting results in a switch in substrate usage from carbohydrates to fat in order to increase survival in the absence of food intake (12). Despite this, the mechanisms regulating the adaptation of skeletal muscle metabolism to changes resulting from the occurrence of a malignancy are unclear.

One of the major enzymes involved in the regulation of metabolic flexibility in mammals is the PDH complex (PDC), a mitochondrial multienzyme complex catalyzing the irreversible conversion of pyruvate to acetyl coenzyme A, located at the nexus of 3 critical metabolic pathways [*i.e.*, glycolysis, tricarboxylic acid (TCA) cycle, and β-oxidation (10)]. This complex is primarily involved in the selection of glucose, fatty acids, and proteins for cellular energy production. PDC activity is mainly regulated by 4 highly specific PDH kinase (PDK) isoenzymes (PDK1, 2, 3, and 4) that can phosphorylate specific serine residues within the α-subunit of the E1 enzyme in PDC (13). Of all the PDK isozymes, PDK1 and PDK3 present a rather limited tissue distribution. However, PDK2 and PDK4 are widely expressed in a range of tissues, such as skeletal muscle, heart, pancreatic islets, liver, and kidneys in humans and rodents. Interestingly, PDK4 seems to be critically involved in the regulation of the cellular energetic metabolism in pancreatic islets and skeletal muscles, which are known for elevated utilization of glucose and high fatty acid–oxidation rates (14, 15). Published data also suggest that PDK4 may regulate tumor proliferation and the response to chemotherapeutics, although the underlying mechanisms have not been fully characterized yet (16–18).

PDK4 was found elevated in skeletal muscle in animal models for the study of cancer, starvation, diabetes, sepsis, or amyotrophic lateral sclerosis (19–25), whereas its pharmacologic inhibition in mice was reported to improve statin-mediated myopathies (26), reduce endotoxaemia-induced muscle protein (24), and attenuate the loss of body weight and fat mass in the presence of a tumor (25). PDK4 has been reported as a key target gene of Forkhead box protein O (FOXO)1, peroxisome proliferator–activated receptor (PPAR)δ or PPARα in response to the signaling mediated by insulin, elevated free fatty acids, or starvation (20, 27–29). However, the

role of PDK4 in direct regulation of skeletal muscle size and function remains unclear. In the present study, we sought to investigate the metabolic link between PDK4 activation and changes in muscle size in the context of cancer-associated cachexia with the ultimate goal of validating the role of PDK4 in the pathogenesis of cachexia. Our findings identified PDK4 as a potential new target for the treatment of cancer-associated muscle disorders.

MATERIALS AND METHODS

Animals

All animal experiments were conducted with the approval of the Institutional Animal Care and Use Committee at the Indiana University School of Medicine, and were in compliance with the *Guidelines for Use and Care of Laboratory Animals* [National Institutes of Health (NIH), Bethesda, MD, USA] and with the ethical standards laid down in the 1964 Declaration of Helsinki and its later amendments. All animals were maintained on a regular 12-h light/dark cycle (light from 8 AM to 8 PM) with free access to food and water during the whole experimental period. For the colon 26 (C26) xenograft model, 8-wk-old CD2F1 male mice (Envigo, Huntingdon, United Kingdom) were used (n = 8). Mice were randomized into 2 groups: control mice inoculated with sterile saline and tumor-bearing animals injected subcutaneously and intrascapularly with 1×10^6 C26 adenocarcinoma cells.

For the metastatic (m)C26 model, 8-wk-old CD2F1 male mice were randomized into sham-treated (serving as controls; n = 8) and tumor-bearing animals (mC26) presenting with intrasplenic injection of 5×10^5 C26 cells in sterile saline (n = 8) (30). For the pirinixic acid (WY-14643) experiment, CD2F1 male mice (n = 8) were randomized into 2 groups—namely, mice receiving a regular chow diet and mice fed a diet (Research Diets, New Brunswick, NJ, USA) supplemented with 0.1% WY-14643 (Selleck Chemicals, Houston, TX, USA) (31). For the ES-2 model of ovarian cancer-induced cachexia, female NSG (nonobese diabetic, severe combined immunodeficiency or interleukin 2 receptor, γ-chain null) immunodeficient mice (*In Vivo* Therapeutics Core Facility, Indiana University Simon Cancer Center, Indianapolis, IN, USA) were randomized into controls (n = 6) and ES-2 hosts (n = 10). The tumor-bearing mice were inoculated intraperitoneally with 1×10^7 ES-2 cells in sterile saline, as previously performed by our group (32).

For the experiments involving the use of chemotherapy, 8-wk-old CD2F1 male mice were used. For each treatment, mice were randomized as follows. Mice treated with vehicle (saline) served as controls (n = 8), whereas the remaining animals were treated with chemotherapy (n = 8). All drugs were purchased from MilliporeSigma (Burlington, MA, USA) unless otherwise specified. The mice administered with Folfiri received a combination of 5-fluorouracil (50 mg/kg), leucovorin (90 mg/kg), and CPT-11 (24 mg/kg, i.p.), twice weekly, for up to 5 wk (33). The animals treated with cisplatin, receiving daily intraperitoneal injections (2.5 mg/kg) for up to 2 wk (34). The animals treated with carboplatin received the drug as weekly intraperitoneal injections (80 mg/kg in sterile saline) for up to 3 wk. The animals were monitored for the entire duration of the experiments. At the time of euthanization, no animals were excluded from the study. Several tissues were collected, weighed, snap frozen in liquid nitrogen, and stored at −80°C for further analyses. The tibialis anterior muscle was frozen in liquid nitrogen–cooled isopentane, mounted in optimal cutting temperature compound (OCT), and stored for morphologic analyses.

Body composition assessment

Body composition [*i.e.*, the quantification of lean (muscle) and fat (adipose) mass] was assessed at baseline and once weekly over the entire duration of the experiments in physically restrained mice by means of an EchoMRI-100 (EchoMRI, Houston, TX, USA) as previously shown by Pin *et al*. (32). Data were expressed as variations over the baseline values.

Grip strength

The evaluation of the whole-body strength in mice was assessed as previously described by Bonetto *et al*. (35). The absolute grip strength (peak force expressed in grams) was recorded by means of a grip strength meter (Columbus Instruments, Columbus, OH, USA). Five measurements were completed, and the top 3 measurements were included in the analysis. In order to avoid habituation, the animals were tested for grip strength no more than once weekly.

Assessment of muscle cross-sectional area

For histology and morphometry of skeletal muscle, 8-μm–thick cryosections of tibialis anterior muscles taken at the midbelly were stained with hematoxylin and

eosin, as reported by Bonetto *et al*. (35). All samples were observed under an Axio Observer.Z1 motorized microscope (Carl Zeiss, Oberkochen, Germany), and images were recorded for morphometric examination. For the analysis of the cross-sectional area (CSA), muscle fibers (n = 300–500/sample) were measured using a Cintiq pen tablet input device (Wacom, Kazo, Japan) and ImageJ (NIH; v.1.43) software (36) as also described by Bonetto *et al*. (35).

Cell lines

Murine C26 cells were provided by Donna McCarthy (Ohio State University, Columbus, OH, USA) and cultured in high-glucose (4.5 g/L) DMEM supplied with 10% fetal bovine serum, 1% glutamine, 1% sodium pyruvate, and 1% penicillin and streptomycin. Cells were maintained in a 5% CO_2, 37°C humidified incubator. Human ES-2 cells were purchased from American Type Culture Collection (ATCC) (CRL-1978; Manassas, VA, USA) and were cultured in McCoy's medium supplied with 10% fetal bovine serum, 1% glutamine, 1% sodium pyruvate, and 1% penicillin and streptomycin in a 5% CO_2, 37°C humidified incubator. Murine C2C12 skeletal myoblasts (ATCC) were grown in high-glucose DMEM supplemented with 10% fetal bovine serum, 100 U/ml penicillin, 100 mg/ml streptomycin, 100 mg/ml sodium pyruvate, and 2 mM L-glutamine and maintained at 37°C in 5% CO_2. Myotubes were generated by exposing the myoblasts to DMEM containing 2% horse serum and replacing the medium every other day for 5 d. In order to determine the effects on myotube size and metabolism dependent on tumor-derived factors, chemotherapy, or WY-14643, C2C12 myotubes were exposed to conditioned medium (CM) and collected from confluent C26 culture plates (25%), Folfiri (50 μg/ml 5-fluorouracil, 10 μg/ ml leucovorin, 20 μg/ml CPT-11), or WY-14643 (50 μM) for up to 48 h, respectively. To study the effects resulting from modulation of PDK4 expression, C2C12 myotubes were infected with 10^7 plaque forming units (PFUs) of the following adenoviral (Ad) constructs made using human recombinant adenovirus serotype 5 constructs, in which green fluorescent protein (GFP) and genes of interest are expressed from separate cytomegalovirus (CMV) promoters: Ad-GFP-mPDK4 (268336), Ad-GFP (1060), Ad-GFP-U6-mPDK4-short hairpin RNA (shRNA) (shADV268336), Ad-GFP-U6-shRNA (scrambled) adenovirus (1122) (Vector Biolabs, Malvern, PA, USA).

Generation of tumor-derived CM

Murine C26 cells were grown in culture medium as described above. Once the cells layers reached >80% confluency, the culture medium was eliminated and replaced with fresh medium containing 10% fetal bovine serum, 1% glutamine, 1% sodium pyruvate, and 1% penicillin and streptomycin. After 48 h, the CM was collected, centrifuged at 1200 rpm for 10 min at 4°C, and stored at −80°C for further studies.

Assessment of myotube size

Cell layers were fixed in ice-cold acetone-methanol and incubated with an anti-myosin heavy chain antibody (MF-20, 1:200; Developmental Studies Hybridoma Bank, Iowa City, IA, USA) and an AlexaFluor 488–labeled secondary antibody (Thermo Fisher Scientific, Waltham, MA, USA). Analysis of myotube size was performed by measuring the minimum diameter of long, multinucleate fibers, avoiding regions of clustered nuclei, on a calibrated image using the ImageJ 1.43 software (36). Three statistical replicates were generated for each experimental condition, and about 250–350 myotubes per replicate were measured. The results of each replicate were then averaged to obtain the final myotube size.

MitoTracker red CMXRos

Mitochondria polarization was determined using the MitoTracker Red CMXRos Selective Probe (Thermo Fisher Scientific). C2C12 myotubes were exposed to 25% CM, collected from confluent C26 culture plates, and subjected to centrifugation to remove cell debris or treated with Folfiri for 48 h. After incubation in a medium without fetal bovine serum, the cells were exposed to medium containing 100 nM MitoTracker for 30 min at 37°C. The cell layers were then exposed to a complete medium containing 3.7% paraformaldehyde for 15 min at 37°C. Images were captured using a fluorescence microscope (Carl Zeiss), and the quantification of the images was performed by using the ImageJ 1.43 software (36).

Western blotting

Total protein extracts were obtained by lysing cell layers or homogenizing 100 mg quadriceps muscle tissue in RIPA buffer (150 mM NaCl, 1.0% NP-40, 0.5% sodium deoxycholate, 0.1% SDS, and 50 mM Tris, pH 8.0) completed with protease (Roche, Basel, Switzerland) and phosphatase (Thermo Fisher Scientific) inhibitor cocktails. Cell debris was removed by centrifugation (15 min, 14,000 *g*) and the supernatant

collected and stored at −80°C. Protein concentration was determined using the bicinchoninic acid (BCA) protein assay method (Thermo Fisher Scientific). Protein extracts (30 μg) were then electrophoresed in 4–15% gradient SDS Criterion TGX precast gels (Bio-Rad, Hercules, CA, USA). Gels were transferred to nitrocellulose membranes (Bio-Rad). Membranes were blocked with Sea Block blocking reagent (Thermo Fisher Scientific) at room temperature for 1 h, followed by an overnight incubation with diluted antibody in Sea Block buffer containing 0.2% Tween 20 at 4°C with gentle shaking. After washing with PBS containing 0.2% Tween 20, the membranes were incubated at room temperature for 1 h with either anti-rabbit IgG (H+L) DyLight 800 or anti-mouse IgG (H+L) DyLight 600 (Cell Signaling Technology, Danvers, MA, USA). Blots were then visualized with Odyssey Infrared Imaging System (Li-Cor Biosciences, Lincoln, NE, USA). Optical density measurements were taken using the Gel-Pro Analyzer software. Antibodies used were optic atrophy protein 1 (OPAI) (80471), Mitofusin 2 (9482), cytochrome *c* (11940), and ubiquitin (3933) (Cell Signaling Technology), PDK4 (ab214938) [Abcam (Cambridge, United Kingdom)], PGC1α (ab3242) (MilliporeSigma), and α-tubulin (12G10; Developmental Studies Hybridoma Bank).

Real-time quantitative PCR

RNA from quadriceps was isolated using the miRNeasy Mini Kit (Qiagen, Germantown, MD, USA) and following the protocol provided by the manufacturer. RNA was quantified using a Synergy H1 Spectrophotometer (BioTek Instruments, Winooski, VT, USA). RNA integrity was checked by electrophoresis on a 1.2% agarose gel containing 0.02 M morpholinopropanesulfonic acid and 18% formaldehyde. Total RNA was reverse transcribed to cDNA using the Verso cDNA Kit (Thermo Fisher Scientific). Transcript levels were measured by real-time PCR (Light Cycler 96; Roche), taking advantage of the TaqMan Gene Expression Assay System (Thermo Fisher Scientific). Expression levels for atrogin-1 (Mm00499523_m1) and MuRF-1 (Mm01185221_m1) were detected. Gene expression was normalized to TATA-binding protein (Mm01277042_m1) levels using the standard $2^{-\Delta Ct}$ methods.

SDH staining

Tibialis anterior cross sections (10 μm) were cut on a cryostat and incubated for 30 min at 37°C with 0.5 mg/ml nitroblue tetrazoliumand, 50 mM Na-succinate, and 0.08 mM phenazine methosulfate in PBS. The slides were then rinsed 3 times in deionized

water, mounted with PBS-glycerol, and photographed using an Axio Observer.Z1 motorized microscope (Carl Zeiss). Entire SDH-stained sections were quantified for integrated density, as well as total, oxidative, and glycolytic fiber number using ImageJ.

PDH and SDH enzymatic activity

The enzymatic activities of PDH and SDH were measured using Colorimetric Assay Kits (MAK051 and MAK197, respectively) from MilliporeSigma according to the manufacturer's instructions. Briefly, 10 mg of skeletal muscle tissue or 1×10^6 C2C12 was homogenized in 100 µl of ice-cold assay buffer then centrifuged, and 10 µl of homogenate was added to 96-well plates. Appropriate reaction mix was added to each of the wells and the product of enzyme reaction, which results in a colorimetric (600 nm for SDH and 450 nm PDH) product proportional to the enzymatic activity. The absorbance was recorded by incubating the plate at 37°C, taking measurements (600 and 450 nm) every 5 min for 30 min.

Extracellular flux analysis

Mitochondrial oxygen consumption rate (OCR) was measured using a Mito-Stress Test Kit in a Seahorse XF Extracellular Flux Analyzer (Agilent Technologies, Santa Clara, CA, USA) according to the manufacturer's instructions. C2C12 myoblasts were plated in an XF cell culture microplate (30.000 cells/cm^2) and then differentiated to myotubes by exposing the myoblasts to DMEM containing 2% horse serum and replacing the medium every other day for 5 d. The cells were then exposed to Ad-GFP-mPDK4 or Ad-GFP (10^7 PFU/ml) for up to 48 h. One hour prior to the assay, the cells were incubated in Seahorse XF Base Medium (Agilent Technologies) containing 1 mM Na-pyruvate, 2 mM glutamine, and 25 mM glucose in a non-CO_2 incubator for 1 h at 37°C. Basal respiration was monitored prior to the addition of 2 µM oligomycin. The OCR values were obtained at baseline and after the addition of 2 µM oligomycin, 1 µM carbonyl cyanide 4-(trifluoromethoxy)phenylhydrazone, and 0.5 µM rotenone. OCR was automatically calculated and recorded by the Seahorse XF software (Agilent Technologies), and data were expressed as picomolars per minute.

Statistical analysis

Results are presented as means ± SD. Significance of the differences was determined

by either unpaired Student's *t* test, or ANOVA followed by Tukey's posttest. Differences were considered significant when $P < 0.05$.

RESULTS

Tumor-derived factors lead to mitochondrial changes and increased PDK4 expression

We evaluated the role of tumor-derived soluble factors in the promotion of derangements consistent with altered energy metabolism and abnormal mitochondrial functioning, similar to what we previously observed in the muscles of C26-bearing mice (8). We exposed mature C2C12 myotubes to either control medium [differentiation medium added with 25% unconditioned medium (UCM)] or differentiation medium added with 25% C26 CM for up to 48 h (**Fig. 1**). The presence of C26 CM resulted in a significant reduction of mitochondria polarization (−14% *vs.* UCM, $P < 0.05$) and was sufficient to cause myotube atrophy (−41% *vs.* UCM, $P < 0.001$) (Fig. 1*A*). Consistent with mitochondrial derangements and a reduced oxidative metabolism in the C2C12 myotubes exposed to tumor CM, PDK4 protein levels were significantly elevated compared with the control (+61%, $P < 0.05$; Fig. 1*B*). Interestingly, C2C12 myotubes exposed to the chemotherapy regimen Folfiri for up to 48 h displayed reduced myofiber size (unpublished results and ref. 33), along with decreased polarized mitochondria (−36% *vs.* vehicle, $P < 0.01$; Supplemental Fig. S1*A*) and markedly increased PDK4 levels (+5.9 folds *vs.* vehicle, $P < 0.001$; Supplemental Fig. S1*B*). These findings further suggest that abnormal mitochondria and an oxidative-to-glycolytic switch in energy metabolism are sufficient to promote muscle atrophy and in line with our previous findings (33).

Growth of the C26 tumor causes reductions of oxidative metabolism consistent with elevated muscle PDK4 levels

Similar to our previously published findings (37), the C26 colon adenocarcinoma caused a progressive loss of body weight (Supplemental Fig. S2*A*), resulting in a significant depletion of body mass (−4.07 g *vs.* control, $P < 0.001$; Supplemental Fig. S2*B*), as well as changes in body composition, consistent with markedly depleted adipose (−50% *vs.* control, $P < 0.001$) and lean tissue mass (−14% *vs.* control, $P < 0.01$; Supplemental Fig. S2*C*). Skeletal muscles appeared significantly smaller in the

tumor hosts, with the quadriceps muscle showing a reduction of ~21% compared with the healthy mice ($P < 0.01$; Supplemental Fig. S2*D*). This is in line with the cachexia-inducing effects due to the growth of the C26 tumor. In order to determine the effect of tumor growth on muscle energy metabolism, we assessed the enzymatic activities of key enzymes regulating the flow of energy substrates through glycolysis and TCA cycle (*i.e.*, PDH and SDH). PDH and SDH activities were markedly reduced compared with the control animals (−65 and −53%, respectively) in the quadriceps muscle of C26 hosts (**Fig. 2*A***), further confirming our and other previous findings as well as supporting the idea that cancer promotes a switch to a muscle metabolism associated with reduced glucose oxidation (8, 38). Keeping in mind that PDH activity is directly regulated by PDKs, we investigated the role of the expression of PDK4, the most relevant muscle isoform, in the skeletal muscle of tumor hosts, similar to what shown in Fig. 1. PDK4 expression in the quadriceps muscle of C26-bearing mice was increased over 5-fold ($P < 0.01$) compared with the control animals (Fig. 2*B*). In order to determine the role of PDK4 in different conditions characterized by severe muscle wasting, we assessed PDK4 expression in multiple animal models of cancer- and chemotherapy-induced cachexia, namely mice with C26 colorectal liver metastases (30) or bearing ES-2 high-grade serous ovarian cancer (32), as well as animals receiving Folfiri (33), carboplatin, or cisplatin (34) (Supplemental Fig. S3). Interestingly, in all cases, the depletion of quadriceps muscle mass (Supplemental Fig. S3*A*) was inversely correlated with PDK4, whose expression resulted dramatically elevated in the cisplatin-treated mice (over 25 folds *vs.* vehicle, $P < 0.001$; Supplemental Fig. S3*B*).

PDK4 drives muscle wasting in C2C12 cultures and animals exposed to WY-14643

In order to investigate the role of elevated PDK4 in the cause of muscle atrophy *per se*, we exposed mature C2C12 myotubes to 50 μM WY-14643, a selective agonist for the PPAR-α, previously shown to induce large increases in PDK4 protein and mRNA in skeletal muscle (20, 39). After 48-h treatment with WY-14643, the myotubes exhibited marked atrophy (−16% *vs.* control, $P < 0.01$; **Fig. 3*A***), also consistent with a 2-fold increase in PDK4 expression (Fig. 3*B*). To further validate our results, we fed normal CD2F1 male mice a diet enriched in 0.1% WY-14643 for up to 3 wk to assess muscle wasting in *in vivo* conditions (**Fig. 4**). Despite similar food intake in both experimental groups (Fig. 4*A*), starting at d 4, the WY-14643–fed animals showed progressive and significant decrease in body mass (Fig. 4*B*), ultimately resulting in

~28% loss of body weight ($P < 0.001$) at time of euthanization when compared with the animals receiving the control diet (Fig. 4*C*). Consistent with the reduction in body weight, WY-14643 administration was also responsible for progressive and dramatic loss of fat tissue and, to a lesser extent, lean mass, as reported in Fig. 4*D*. In line with changes in the amount of lean tissue, skeletal muscle atrophy was evident in the animals receiving WY-14643 in their food (Fig. 4*E*), consistent with marked skeletal muscle atrophy, as suggested by the reduction in tibialis anterior (−21% *vs.* control, $P < 0.001$), gastrocnemius (−30% *vs.* control, $P < 0.001$), and quadriceps mass (−36% *vs.* control, $P < 0.001$; Fig. 4*F*). The decrease in muscle mass was also reflected in markedly reduced muscle CSA of the tibialis anterior muscle (−24% *vs.* control; $P < 0.01$; **Fig. 5*A, B***). The SDH staining in the tibialis anterior muscle sections also revealed overall reduced oxidative metabolism (Fig. 5*A, C*), along with reduced number of oxidative fibers and increase in fibers endowed with more glycolytic metabolism (Fig. 5*D*). Consistent with the reduced oxidative metabolism, decreased PDH (−35% *vs.* control; $P < 0.05$) and SDH (−21% *vs.* controls, $P < 0.05$) enzymatic activities were also detected (Fig. 5*E*). In order to investigate the relationship between changes in energy metabolism and altered mitochondrial homeostasis in the WY-14643–fed animals, we assessed the expression of known markers of mitochondrial biogenesis and fusion, in line with our previous findings (32, 40). As shown in Fig. 5*F*, elevated PDK4 expression (+128% *vs.* control, $P < 0.001$) was accompanied by markedly reduced PGC1α (−38% *vs.* control, $P < 0.001$), OPA1 (−37% *vs.* controls, $P < 0.05$), Mitofusin 2 (−36% *vs.* controls, $P < 0.001$) and cytochrome c (−43% *vs.* controls, $P < 0.01$). Notably, atrogin-1 and MuRF-1, ubiquitin ligases notoriously overexpressed in association with muscle atrophy (41, 42), were highly expressed in the skeletal muscle of animals receiving WY-14643 (+228%, $P < 0.001$ for atrogin-1 and +79%, $P < 0.05$ for MuRF-1) when compared with the control mice (Fig. 5*G*), suggesting that the observed muscle phenotype may result from activated skeletal muscle hypercatabolism.

High PDK4 induces myofiber atrophy and alterations to the energy metabolism

In order to define the effect of direct modulation of PDK4 levels on the promotion of muscle atrophy, mature C2C12 myotubes were infected with an Ad construct for murine PDK4. We found that elevated PDK4 (+24-fold *vs*. Ad-GFP, $P < 0.001$) was associated with altered expression of mitochondrial markers, such as OPA1 (−43% *vs*. Ad-GFP, $P < 0.05$) and Mitofusin 2 (−42% *vs*. Ad-GFP, $P < 0.05$; **Fig. 6*A***). Interestingly, the C2C12 overexpressing PDK4 also showed elevated levels of

ubiquitinated proteins (+2.5-fold *vs*. Ad-GFP, $P < 0.05$), further supporting the idea that high PDK4 directly correlates with exacerbated muscle hypercatabolism (Fig. 6*D*). This is analogous to the scenario described in the skeletal muscle of WY-14643-treated animals. As shown in Fig. 6*B*, PDK4 overexpression was sufficient to cause marked myotube atrophy (−24% *vs*. Ad-GFP, $P < 0.001$), as well as metabolic derangements accompanied by reduced PDH (−22% *vs*. Ad-GFP, $P < 0.01$) and SDH (−11% *vs*. Ad-GFP, $P < 0.05$) activities (Fig. 6*C*). Elevated PDK4 was also directly responsible for altered mitochondrial respiration (Fig. 6*D*). Overall, the analysis of the oxygen consumption rate (OCR) showed decreased basal respiration (BR; −17%, $P < 0.01$), maximal respiration (MR; −25%, $P < 0.05$), spare respiratory capacity (SRC; −27%, $P < 0.05$) and increased proton leak (PL; $P < 0.01$) compared to Ad-GFP.

PDK4 blockade prevents myotube atrophy in C2C12 cultures exposed to C26 CM

We performed a blockade of PDK4 in C2C12 myotubes by means of Ad-GFP-shPDK4 in order to validate PDK4 as a key regulator of muscle size (**Fig. 7**). Similar to Fig. 1, treatment of myotubes with 25% C26 CM for up to 48 h induces significant atrophy (−40%, $P < 0.001$) when compared with cultures exposed to UCM alone (Fig. 7*A*). Similarly, cell layers exposed to C26 CM and infected with a control virus (Ad-GFP-shScr) showed a similar degree of atrophy (−39% *vs.* Ad-shRNA scrambled (Ad-shScr) + UCM, $P < 0.001$). However, C2C12 cultures infected with Ad-shPDK4 and exposed to C26 CM displayed a larger myotube size (+43% *vs.* Ad-shScr + C26 CM, $P < 0.001$), whereas there was no statistical difference when compared with the Ad-shPDK4–infected myotubes (ANOVA: $P < 0.0001$; $F = 41.01$; degree of freedom of the numerator (Dfn) = 5; degree of freedom of the denominator (Dfd) = 58) (Fig. 7*A*). This is consistent with reduced PDK4 protein levels in cultures exposed to Ad-shPDK4 and C26 CM (Fig. 7*B*). Similarly, PDH activity was almost completely restored in the myotubes infected with Ad-shPDK4 and exposed to C26 CM (ANOVA: $P < 0.0001$; $F = 91.34$; DFn = 3; Dfd = 8) (Fig. 7*C*). These data suggest that PDK4 blockade preserves myotube size and prevents metabolic derangements in the presence of tumor-derived factors.

DISCUSSION

In the present study, we reported that PDK4 is consistently up-regulated in atrophic skeletal muscle following the development of cancer. In a similar manner, we also showed that PDK4 is highly expressed in the muscle of animals exposed to

chemotherapeutics, such as Folfiri, carboplatin, and cisplatin, in association with severe muscle loss (33, 34). Others have previously shown elevated PDK4 expression concurrently with the depletion of muscle mass; however, no mechanistic data have been presented thus far. Indeed, PDK4 was found elevated in muscle along with the onset of experimental cancer, starvation, diabetes, sepsis, or amyotrophic lateral sclerosis in animal models (19–26). Moreover, PDK4 hyperexpression in cardiac muscle was shown to exacerbate the cardiomyopathy induced by abnormal activation of the calcineurin pathway in response to stress conditions, although its overexpression *per se* was not sufficient to cause changes in heart size (43). Our observation, that PDK4 overexpression is sufficient to cause muscle atrophy, represents the first evidence of a direct interaction between PDK4 and the regulation of muscle size.

Cancer growth drives an overall persistent imbalance in the use of energy substrates, often resulting in severe metabolic derangements (8, 40). We and others have previously investigated some of the mechanisms involved in promoting the metabolic dysfunctions frequently involved in the occurrence of cancer-induced cachexia (8, 33, 44, 45). Along this line, malfunctioning of energy metabolism was shown to promote depletion of muscle mass and strength in cachectic mice bearing Lewis lung carcinoma (46). Evidence from our group showed that animals bearing the C26 colorectal adenocarcinoma and mice chronically exposed to the chemotherapy regimen, Folfiri, present reduced levels of proteins related to oxidative phosphorylation, TCA cycle, and glycolysis in their skeletal muscle (40). In addition, we recently showed that the growth of the C26 colorectal cancer, along with loss of body and muscle mass, contributes to increased systemic glucose demand, unique aberrations in TCA cycle, and β-oxidation pathways as well as conspicuous elevation in LDL particles (8). Specifically, our comprehensive metabolomics analysis revealed several tumor-derived abnormalities in the TCA cycle functioning, primarily consistent with significant reductions in the circulating levels of citrate and succinate, decreased muscle PDH and SDH enzymatic activities, and reduced production of muscle energy metabolites, such as ATP and creatine phosphate (8). These findings were also consistent with an increase in the number of fibers endowed with a glycolytic metabolism and with changes in mitochondrial homeostasis, as previously described by Pin *et al*. (38), in the skeletal muscle of animals bearing cancer or exposed to chemotherapy (33).

In line with our previous data, inactivation of PDH is prevalent regardless of the

nature of the metabolic changes associated with muscle atrophy (8). In skeletal muscle tissue, PDH regulates the entry of pyruvate into the TCA cycle and catalyzes the irreversible oxidative decarboxylation of pyruvate within the mitochondria of mammalian cells, thereby generating NADH, acetyl coenzyme A, and CO_2. The flux of energy substrates through PDH is tightly regulated by phosphorylation and dephosphorylation cycles by means of PDKs and PDH phosphatases. PDKs are expressed across different tissues in mammals, and their expression is transcriptionally regulated in response to a plethora of stimuli (47). Indeed, although PDK1 and PDK3 expression is directly stimulated by hypoxia-inducible factor 1α in conditions of hypoxia or in cancer cells, nutritional factors and hormones mainly control PDK2 and PDK4 functions (48, 49). In particular, PDK4 was shown to play a critical role in regulating the energy metabolism in highly oxidative tissues, such as pancreatic islets and skeletal muscles (14, 15). In this context, our observations are the first to provide evidence that high PDK4 expression not only affects the overall metabolic flexibility but also promotes changes in skeletal muscle size.

Of interest, PDK4, whose functions are closely correlated to the regulation of glucose consumption and oxidation in skeletal muscle, liver, kidney, and heart, has been shown to respond to stimulation mediated by transcription factors such as FOXO1 and FOXO3 and several nuclear hormone receptors, such as PPARs, glucocorticoid receptors, thyroid hormone receptors, and estrogen-related receptors (50). Moreover, proinflammatory mediators, such as IL-6 and TGF-β, have also been associated with PDK4-induced regulation of energy metabolism, although the mechanisms responsible for these events remain unclear (18, 51). All these signaling factors have been previously correlated with the occurrence of muscle atrophy in both experimental and clinical cachexia.

FOXO1 and FOXO3 are known to be key factors of muscle energy homeostasis involved in the regulation of glycolytic and lipolytic flux as well mitochondrial metabolism. FOXO1 is an important regulator of glucose metabolism in skeletal muscle primarily because of its ability to bind directly to the promoter region of the PDK4 gene, thus promoting its expression during conditions associated with energy deprivation (50). FOXO1 has also been involved in the regulation of supply and oxidation of fatty acids (52). Along with FOXO3, FOXO1 operates downstream of PI3K and Akt signaling and has been closely associated with the activation of 2 major proteolytic systems in skeletal muscle—namely, the ubiquitin-proteasome and the autophagy-lysosomal pathways (42, 53). Indeed, FOXO-dependent transcription has

been centrally involved in controlling a network of procachectic genes associated with the onset of cancer-induced muscle wasting (54), and the role of FOXO1 and 3 in promoting the loss of muscle proteins *via* hyperactivation of the ubiquitin-proteasome system has been extensively characterized (42). In the present study, in conditions of myofiber atrophy and high PDK4 expression, we observed enhanced protein catabolism as suggested by either elevated levels of ubiquitin ligases atrogin-1 and MuRF1 or by increased protein ubiquitination. Interestingly, correction of energy metabolism by PDK4 pharmacologic inhibition proved beneficial in conditions characterized by FOXO1 up-regulation, such as the case of statin-induced myopathies or right ventricular hypertrophy that follows the onset of pulmonary hypertension (26, 55). Altogether, these observations strengthen the idea that FOXO factors may participate in causing muscle wasting primarily by activating downstream effectors involved in the regulation of both energy metabolism and muscle protein content.

PPAR transcription factors, including PPARα, PPARβ/δ, and PPARγ, are known to regulate the expression of genes involved in several metabolic processes. In this regard, PPARα promotes ketogenesis and fatty-acid oxidation in conditions of fasting and was shown to activate expression of PDKs. PPARα has also been shown to directly activate lipolysis, and PPARα pharmacologic agonists have been studied for their ability to improve obesity-induced metabolic abnormalities (56). Interestingly, free fatty acids are well-known endogenous PPARα agonists, thereby indirectly causing elevations in PDK expression in conditions of fasting or diabetes (39, 57). PDKs have also been indicated as primary PPARδ target genes in humans based on several PPRE recognition sequences in their promoters (58), and PDK4 expression has been shown to increase upon direct stimulation mediated by PPAR-δ agonists in HepG2 hepatocellular carcinoma cells (59). In addition to enhanced expression of PDKs, PPAR-δ activation was also found to increase the expression of genes involved in the uptake and oxidation of lipids in skeletal muscle. A functional interaction between PPARδ, the lipid transporter CD36, and PDK4 has been validated in myofibers. Based on this model, CD36 mediates the uptake of fatty acids and leads to activation of PPARδ and, in turn, increased expression of PDK4 (28).

In our studies, conducted in both *in vitro* and *in vivo* conditions, the PPAR-α pharmacologic agonist WY-14643 drove progressive depletion of muscle atrophy and fat stores as well as reduced oxidative metabolism associated with elevated muscle PDK4 protein expression. Similar findings reported by our group showed that growth

of the C26 tumor not only resulted in marked muscle atrophy but also in severe wasting of adipose tissue and hyperlipidemia as also evidenced by dramatically elevated levels of LDL particles (8, 37). The latter could potentially explain the described muscle phenotype, especially keeping in mind that excessive oxidation of fatty acids was recently described as a major driver of muscle depletion in cancer cachexia (60). However, we recently showed that the levels of intermediates of the β-oxidation were reduced in the plasma of C26 hosts, suggesting reduced oxidation of fatty acids in this model of cachexia. This may also be a result of incomplete fatty-acid oxidation due to the tumor-associated muscle mitochondrial deficits as also previously described (38, 40). This may lead to the buildup of intermediates of fatty-acid oxidation and elevations in PDK4 expression (61).

PDK4 involvement in the control of tumor proliferation and in the response to anticancer treatments has also been proposed (16–18). In a seminal study, Warburg *et al.* (62) observed that tumors generally exhibit high-glucose utilization compared with normal tissue. More recently, several oncogenes and tumor suppressors were also found to directly control glycolysis and energy production in tumor cells (63). PDKs take part in this phenomenon and may indirectly support cellular transformation and apoptosis resistance in cancer. In particular, PDK4 was previously shown to regulate the cAMP response element-binding protein–Ras homolog enriched in brain–mammalian target of rapamycin signaling cascade, thereby promoting tumorigenesis in various cancer cell lines (16). Decreased methylation of the PDK4 gene, leading to elevated expression of this kinase, was also found in colon cancers compared with normal colon mucosa, thus further supporting the idea that PDK4 plays a role in cancer progression and proliferation (64). Based on this evidence, PDK4 has been investigated as a putative target for cancer treatment, and blockade of PDK4 was shown to suppress tumor proliferation by increasing glucose oxidation and promoting higher levels of reactive oxygen species, thereby also suggesting that metabolic changes are sufficient to rapidly neutralize cell proliferation in cancer cells (17). Similarly, PDK4 was reported elevated in association with TGF-β–induced chemoresistance, and its inhibition proved beneficial in sensitizing colorectal cancer cells to 5-fluorouracil, thus suggesting that PDK4 may also represent a therapeutic option to overcome drug resistance in cancer cells (18).

Our work showed that the blockade of PDK4 is able to restore the metabolic abnormalities and preserve fiber size in myotubes exposed to tumor-derived CM. Our

evidence is also supported by previous attempts to modulate PDK4 to improve the muscle phenotype. Indeed, PDK4 pharmacologic inhibition by the administration of dichloroacetate was reported to improve statin-mediated myopathies by correcting the metabolic flux and abolishing FOXO-mediated protein breakdown (26). In a similar manner, rosiglitazone administration to LPS-injected rats induced suppression of PDK4 expression and contributed to reduce endotoxaemia-induced muscle protein loss (24). The same agent was able to attenuate the loss of fat as well as to normalize PDK4 and glucose oxidation in the skeletal muscle of early-stage C26 hosts. Conversely, only a modest improvement in adipose tissue mass was observed in late-stage tumor hosts, thus further supporting the idea that early diagnosis of cachexia is critical to attempt therapeutic interventions for the correction of cancer-associated muscle wasting (25).

In summary, our present study reports evidence of an association among elevated PDK4 protein expression, metabolic abnormalities, and muscle atrophy in cancer cachexia. Our mechanistic observations suggest that PDK4 not only is sufficient to induce shrinkage of C2C12 myotubes but also is sufficient for muscle atrophy to occur. Overall, our findings support a novel role for PDK4 in the control of muscle size in cancer states or following chemotherapy treatment. PDK4 may represent a target for the identification of novel therapeutic strategies for the treatment of cancer-associated cachexia. Keeping in mind its protumorigenic effects, our results also provide a foundation for investigating the potentially beneficial effects associated with PDK4 pharmacologic inhibition alone or in combination with anticancer therapies.

Supplementary Material

This article includes supplemental data. Please visit *http://www.fasebj.org* to obtain this information.

ACKNOWLEDGMENTS

The authors thank the Cancer Center at Indiana University (IU) School of Medicine funded by the IU Simon Cancer Center Support Grant (P30CA082709) for the use of the *In Vivo* Therapeutics Core Facility, which generated the NSG mice used in this study. The 12G10 anti-tubulin mAb developed by J. Frankel and E. M. Nelson (University of Iowa, Iowa City, IA, USA) and the MF-20 anti-myosin heavy chain

antibody developed by Donald A. Fischman (Cornell University, Ithaca, NY, USA) were obtained from the Developmental Studies Hybridoma Bank, created by the U.S. National Institutes of Health, National Institute of Child Health, and maintained at the Department of Biology at The University of Iowa. The authors thank John Spence, Ph.D. for contributions in editing the manuscript, and Teresa A. Zimmers, Ph.D. (both from the IU School of Medicine) for allowing access to the equipment for *in vivo* characterization of cachexia. This study was supported by the Department of Surgery and the Department of Otolaryngology–Head and Neck Surgery at IU, and by grants from the V Foundation for Cancer Research (V2017-021 to A.B.), the American Cancer Society (Research Scholar Grant 132013-RSG-18-010-01-CCG to A.B.), the IU Simon Cancer Center (Associate Member Pilot Funding Mechanism to A.B.), the Indiana Clinical and Translational Sciences Institute (Core Pilot Grant UL1TR001108 to T.M.O. and A.B.), and the Showalter Research Trust (to A.B.). The authors declare no conflicts of interest.

Glossary

Ad	adenoviral
Ad-shScr	Ad-shRNA scrambled
C26	colon 26
CM	conditioned medium
CMV	cytomegalovirus
CSA	cross-sectional area
FOXO	Forkhead box protein O
GFP	green fluorescent protein
OCR	oxygen consumption rate

OPA1	optic atrophy protein 1
PDC	PDH complex
PDH	pyruvate dehydrogenase
PDK	PDH kinase
PPAR	peroxisome proliferator–activated receptor
SDH	succinate dehydrogenase
shRNA	short hairpin RNA
TCA	tricarboxylic acid
UCM	unconditioned medium
WY-14643	pirinixic acid

Footnotes

This article includes supplemental data. Please visit http://www.fasebj.org to obtain this information.

AUTHOR CONTRIBUTIONS

F. Pin, T. M. O'Connell, and A. Bonetto conceived and designed the experiments; F. Pin, L. J. Novinger, J. R. Huot, and A. Bonetto performed the *in vitro* and *in vivo* experiments, the body composition assessment, the muscle function analysis, and the molecular characterization of cachexia; and F. Pin, R. A. Harris, M. E. Couch, T. M. O'Connell, and A. Bonetto wrote and edited the manuscript.

REFERENCES

1. Fearon K., Arends J., Baracos V. (2013) Understanding the mechanisms and treatment options in cancer cachexia. *Nat. Rev. Clin. Oncol.* 10, 90–99 [PubMed: 23207794]

2. Fearon K. C., Glass D. J., Guttridge D. C. (2012) Cancer cachexia: mediators, signaling, and metabolic pathways. *Cell Metab.* 16, 153–166 [PubMed: 22795476]

3. Skipworth R. J., Stewart G. D., Dejong C. H., Preston T., Fearon K. C. (2007) Pathophysiology of cancer cachexia: much more than host-tumour interaction? *Clin. Nutr.* 26, 667–676 [PubMed: 17507116]

4. Bossola M., Muscaritoli M., Costelli P., Bellantone R., Pacelli F., Busquets S., Argilès J., Lopez-Soriano F. J., Civello I. M., Baccino F. M., Rossi Fanelli F., Doglietto G. B. (2001) Increased muscle ubiquitin mRNA levels in gastric cancer patients. *Am. J. Physiol. Regul. Integr. Comp. Physiol.* 280, R1518–R1523 [PubMed: 11294777]

5. He W. A., Calore F., Londhe P., Canella A., Guttridge D. C., Croce C. M. (2014) Microvesicles containing miRNAs promote muscle cell death in cancer cachexia via TLR7. *Proc. Natl. Acad. Sci. USA* 111, 4525–4529 [PMCID: PMC3970508] [PubMed: 24616506]

6. White J. P., Baltgalvis K. A., Puppa M. J., Sato S., Baynes J. W., Carson J. A. (2011) Muscle oxidative capacity during IL-6-dependent cancer cachexia. *Am. J. Physiol. Regul. Integr. Comp. Physiol.* 300, R201–R211 [PMCID: PMC3043802] [PubMed: 21148472]

7. Johns N., Stephens N. A., Fearon K. C. (2013) Muscle wasting in cancer. *Int. J. Biochem. Cell Biol.* 45, 2215–2229 [PubMed: 23770121]

8. Pin F., Barreto R., Couch M. E., Bonetto A., O'Connell T. M. (2019) Cachexia induced by cancer and chemotherapy yield distinct perturbations to energy metabolism. [E-pub ahead of print] *J. Cachexia Sarcopenia Muscle* [PMCID: PMC6438345] [PubMed: 30680954]

9. Kelley D. E., Mandarino L. J. (2000) Fuel selection in human skeletal muscle in insulin resistance: a reexamination. *Diabetes* 49, 677–683 [PubMed: 10905472]

10. Harris R. A., Bowker-Kinley M. M., Huang B., Wu P. (2002) Regulation of the activity of the pyruvate dehydrogenase complex. *Adv. Enzyme Regul.* 42, 249–259 [PubMed: 12123719]

11. Peters S. J. (2003) Regulation of PDH activity and isoform expression: diet and exercise. *Biochem. Soc. Trans.* 31, 1274–1280 [PubMed: 14641042]

12. Watt M. J., Heigenhauser G. J., Dyck D. J., Spriet L. L. (2002) Intramuscular triacylglycerol, glycogen and acetyl group metabolism during 4 h of moderate exercise in man. *J. Physiol.* 541, 969–978 [PMCID: PMC2290362] [PubMed: 12068055]

13. Gudi R., Bowker-Kinley M. M., Kedishvili N. Y., Zhao Y., Popov K. M. (1995) Diversity of the pyruvate dehydrogenase kinase gene family in humans. *J. Biol. Chem.* 270, 28989–28994 [PubMed: 7499431]

14. Holness M. J., Sugden M. C. (2003) Regulation of pyruvate dehydrogenase complex activity by reversible phosphorylation. *Biochem. Soc. Trans.* 31, 1143–1151 [PubMed: 14641014]

15. Sugden M. C., Holness M. J. (2006) Mechanisms underlying regulation of the expression and activities of the mammalian pyruvate dehydrogenase kinases. *Arch. Physiol. Biochem.* 112, 139–149 [PubMed: 17132539]

16. Liu Z., Chen X., Wang Y., Peng H., Wang Y., Jing Y., Zhang H. (2014) PDK4 protein promotes tumorigenesis through activation of cAMP-response element-binding protein (CREB)-Ras homolog enriched in brain (RHEB)-mTORC1 signaling cascade. *J. Biol. Chem.* 289, 29739–29749 [PMCID: PMC4207987] [PubMed: 25164809]

17. Srivastava N., Kollipara R. K., Singh D. K., Sudderth J., Hu Z., Nguyen H., Wang S., Humphries C. G., Carstens R., Huffman K. E., DeBerardinis R. J., Kittler R. (2014) Inhibition of cancer cell proliferation by PPARγ is mediated by a metabolic switch that increases reactive oxygen species levels. *Cell Metab.* 20, 650–661 [PMCID: PMC4191999] [PubMed: 25264247]

18. Zhang Y., Zhang Y., Geng L., Yi H., Huo W., Talmon G., Kim Y. C., Wang S. M., Wang J. (2016) Transforming growth factor β mediates drug resistance by regulating the expression of pyruvate dehydrogenase kinase 4 in colorectal cancer. *J. Biol. Chem.* 291, 17405–17416 [PMCID: PMC5016137] [PubMed: 27330076] Retracted

19. Jeoung N. H., Wu P., Joshi M. A., Jaskiewicz J., Bock C. B., Depaoli-Roach A. A., Harris R. A. (2006) Role of pyruvate dehydrogenase kinase isoenzyme 4 (PDHK4) in glucose homoeostasis during starvation. *Biochem. J.* 397, 417–425 [PMCID: PMC1533314] [PubMed: 16606348]

20. Wu P., Peters J. M., Harris R. A. (2001) Adaptive increase in pyruvate dehydrogenase kinase 4 during starvation is mediated by peroxisome proliferator-activated receptor alpha. *Biochem. Biophys. Res. Commun.* 287, 391–396 [PubMed: 11554740]

21. Kim Y. I., Lee F. N., Choi W. S., Lee S., Youn J. H. (2006) Insulin regulation of skeletal muscle PDK4 mRNA expression is impaired in acute insulin-resistant states. *Diabetes* 55, 2311–2317 [PubMed: 16873695]

22. Fuster G., Busquets S., Ametller E., Olivan M., Almendro V., de Oliveira C. C., Figueras M., López-Soriano F. J., Argilés J. M. (2007) Are peroxisome proliferator-activated receptors involved in skeletal muscle wasting during experimental cancer cachexia? Role of beta2-adrenergic agonists. *Cancer Res.* 67, 6512–6519 [PubMed: 17616713]

23. Palamiuc L., Schlagowski A., Ngo S. T., Vernay A., Dirrig-Grosch S., Henriques A., Boutillier A. L., Zoll J., Echaniz-Laguna A., Loeffler J. P., René F. (2015) A metabolic switch toward lipid use in glycolytic muscle is an early pathologic event in a mouse model of amyotrophic lateral sclerosis. *EMBO Mol. Med.* 7, 526–546 [PMCID: PMC4492815] [PubMed: 25820275]

24. Crossland H., Constantin-Teodosiu D., Gardiner S. M., Greenhaff P. L. (2017) Peroxisome proliferator-activated receptor γ agonism attenuates endotoxaemia-induced muscle protein loss and lactate accumulation in rats. *Clin. Sci. (Lond.)* 131, 1437–1447 [PubMed: 28536293]

25. Asp M. L., Tian M., Kliewer K. L., Belury M. A. (2011) Rosiglitazone delayed weight loss and anorexia while attenuating adipose depletion in mice with cancer cachexia. *Cancer Biol. Ther.* 12, 957–965 [PMCID: PMC3280914] [PubMed: 22104958]

26. Mallinson J. E., Constantin-Teodosiu D., Glaves P. D., Martin E. A., Davies W. J., Westwood F. R., Sidaway J. E., Greenhaff P. L. (2012) Pharmacological activation of the pyruvate dehydrogenase complex reduces statin-mediated upregulation of FOXO gene targets and protects against statin myopathy in rodents. *J. Physiol.* 590, 6389–6402 [PMCID: PMC3533200] [PubMed: 23045346]

27. Constantin-Teodosiu D., Constantin D., Stephens F., Laithwaite D., Greenhaff P. L. (2012) The role of FOXO and PPAR transcription factors in diet-mediated inhibition of PDC activation and carbohydrate oxidation during exercise in humans and the role of pharmacological activation of PDC in overriding these changes. *Diabetes* 61, 1017–1024 [PMCID: PMC3331777] [PubMed: 22315317]

28. Nahlé Z., Hsieh M., Pietka T., Coburn C. T., Grimaldi P. A., Zhang M. Q., Das D., Abumrad N. A. (2008) CD36-dependent regulation of muscle FoxO1 and PDK4 in the PPAR delta/beta-mediated adaptation to metabolic stress. *J. Biol. Chem.* 283, 14317–14326 [PMCID: PMC2386936] [PubMed: 18308721]

29. Furuyama T., Kitayama K., Yamashita H., Mori N. (2003) Forkhead transcription factor FOXO1 (FKHR)-dependent induction of PDK4 gene expression in skeletal muscle during energy deprivation. *Biochem. J.* 375, 365–371 [PMCID: PMC1223677] [PubMed: 12820900]

30. Murphy K. T., Struk A., Malcontenti-Wilson C., Christophi C., Lynch G. S. (2013) Physiological characterization of a mouse model of cachexia in colorectal liver metastases. *Am. J. Physiol. Regul. Integr. Comp. Physiol.* 304, R854–R864 [PubMed: 23485871]

31. Huang B., Wu P., Bowker-Kinley M. M., Harris R. A. (2002) Regulation of pyruvate dehydrogenase kinase expression by peroxisome proliferator-activated receptor-alpha ligands, glucocorticoids, and insulin. *Diabetes* 51, 276–283 [PubMed: 11812733]

32. Pin F., Barreto R., Kitase Y., Mitra S., Erne C. E., Novinger L. J., Zimmers T. A., Couch M. E.,

Bonewald L. F., Bonetto A. (2018) Growth of ovarian cancer xenografts causes loss of muscle and bone mass: a new model for the study of cancer cachexia. *J. Cachexia Sarcopenia Muscle* 9, 685–700 [PMCID: PMC6104117] [PubMed: 30009406]

33. Barreto R., Waning D. L., Gao H., Liu Y., Zimmers T. A., Bonetto A. (2016) Chemotherapy-related cachexia is associated with mitochondrial depletion and the activation of ERK1/2 and p38 MAPKs. *Oncotarget* 7, 43442–43460 [PMCID: PMC5190036] [PubMed: 27259276]

34. Chen J. A., Splenser A., Guillory B., Luo J., Mendiratta M., Belinova B., Halder T., Zhang G., Li Y. P., Garcia J. M. (2015) Ghrelin prevents tumour- and cisplatin-induced muscle wasting: characterization of multiple mechanisms involved. *J. Cachexia Sarcopenia Muscle* 6, 132–143 [PMCID: PMC4458079] [PubMed: 26136189]

35. Bonetto A., Andersson D. C., Waning D. L. (2015) Assessment of muscle mass and strength in mice. *Bonekey Rep.* 4, 732 [PMCID: PMC4549925] [PubMed: 26331011]

36. Schneider C. A., Rasband W. S., Eliceiri K. W. (2012) NIH image to imageJ: 25 years of image analysis. *Nat. Methods* 9, 671–675 [PMCID: PMC5554542] [PubMed: 22930834]

37. Bonetto A., Aydogdu T., Jin X., Zhang Z., Zhan R., Puzis L., Koniaris L. G., Zimmers T. A. (2012) JAK/STAT3 pathway inhibition blocks skeletal muscle wasting downstream of IL-6 and in experimental cancer cachexia. *Am. J. Physiol. Endocrinol. Metab.* 303, E410–E421 [PMCID: PMC3423125] [PubMed: 22669242]

38. Pin F., Busquets S., Toledo M., Camperi A., Lopez-Soriano F. J., Costelli P., Argilés J. M., Penna F. (2015) Combination of exercise training and erythropoietin prevents cancer-induced muscle alterations. *Oncotarget* 6, 43202–43215 [PMCID: PMC4791226] [PubMed: 26636649]

39. Wu P., Inskeep K., Bowker-Kinley M. M., Popov K. M., Harris R. A. (1999) Mechanism responsible for inactivation of skeletal muscle pyruvate dehydrogenase complex in starvation and diabetes. *Diabetes* 48, 1593–1599 [PubMed: 10426378]

40. Barreto R., Mandili G., Witzmann F. A., Novelli F., Zimmers T. A., Bonetto A. (2016) Cancer and chemotherapy contribute to muscle loss by activating common signaling pathways. *Front. Physiol.* 7, 472 [PMCID: PMC5070123] [PubMed: 27807421]

41. Lecker S. H., Jagoe R. T., Gilbert A., Gomes M., Baracos V., Bailey J., Price S. R., Mitch W. E., Goldberg A. L. (2004) Multiple types of skeletal muscle atrophy involve a common program of changes in gene expression. *FASEB J.* 18, 39–51 [PubMed: 14718385]

42. Sandri M., Sandri C., Gilbert A., Skurk C., Calabria E., Picard A., Walsh K., Schiaffino S., Lecker S. H., Goldberg A. L. (2004) Foxo transcription factors induce the atrophy-related ubiquitin ligase atrogin-

1 and cause skeletal muscle atrophy. *Cell* 117, 399–412 [PMCID: PMC3619734] [PubMed: 15109499]

43. Zhao G., Jeoung N. H., Burgess S. C., Rosaaen-Stowe K. A., Inagaki T., Latif S., Shelton J. M., McAnally J., Bassel-Duby R., Harris R. A., Richardson J. A., Kliewer S. A. (2008) Overexpression of pyruvate dehydrogenase kinase 4 in heart perturbs metabolism and exacerbates calcineurin-induced cardiomyopathy. *Am. J. Physiol. Heart Circ. Physiol.* 294, H936–H943 [PubMed: 18083902]

44. Fearon K., Strasser F., Anker S. D., Bosaeus I., Bruera E., Fainsinger R. L., Jatoi A., Loprinzi C., MacDonald N., Mantovani G., Davis M., Muscaritoli M., Ottery F., Radbruch L., Ravasco P., Walsh D., Wilcock A., Kaasa S., Baracos V. E. (2011) Definition and classification of cancer cachexia: an international consensus. *Lancet Oncol.* 12, 489–495 [PubMed: 21296615]

45. Petruzzelli M., Wagner E. F. (2016) Mechanisms of metabolic dysfunction in cancer-associated cachexia. *Genes Dev.* 30, 489–501 [PMCID: PMC4782044] [PubMed: 26944676]

46. Tzika A. A., Fontes-Oliveira C. C., Shestov A. A., Constantinou C., Psychogios N., Righi V., Mintzopoulos D., Busquets S., Lopez-Soriano F. J., Milot S., Lepine F., Mindrinos M. N., Rahme L. G., Argiles J. M. (2013) Skeletal muscle mitochondrial uncoupling in a murine cancer cachexia model. *Int. J. Oncol.* 43, 886–894 [PMCID: PMC6903904] [PubMed: 23817738]

47. Bowker-Kinley M. M., Davis W. I., Wu P., Harris R. A., Popov K. M. (1998) Evidence for existence of tissue-specific regulation of the mammalian pyruvate dehydrogenase complex. *Biochem. J.* 329, 191–196 [PMCID: PMC1219031] [PubMed: 9405293]

48. Kim J. W., Tchernyshyov I., Semenza G. L., Dang C. V. (2006) HIF-1-mediated expression of pyruvate dehydrogenase kinase: a metabolic switch required for cellular adaptation to hypoxia. *Cell Metab.* 3, 177–185 [PubMed: 16517405]

49. Spriet L. L., Tunstall R. J., Watt M. J., Mehan K. A., Hargreaves M., Cameron-Smith D. (2004) Pyruvate dehydrogenase activation and kinase expression in human skeletal muscle during fasting. *J. Appl. Physiol. (1985)* 96, 2082–2087 [PubMed: 14966024]

50. Kwon H. S., Huang B., Unterman T. G., Harris R. A. (2004) Protein kinase B-alpha inhibits human pyruvate dehydrogenase kinase-4 gene induction by dexamethasone through inactivation of FOXO transcription factors. *Diabetes* 53, 899–910 [PubMed: 15047604]

51. Gudiksen A., Bertholdt L., Vingborg M. B., Hansen H. W., Ringholm S., Pilegaard H. (2017) Muscle interleukin-6 and fasting-induced PDH regulation in mouse skeletal muscle. *Am. J. Physiol. Endocrinol. Metab.* 312, E204–E214 [PubMed: 28028037]

52. An D., Rodrigues B. (2006) Role of changes in cardiac metabolism in development of diabetic

cardiomyopathy. *Am. J. Physiol. Heart Circ. Physiol.* 291, H1489–H1506 [PubMed: 16751293]

53. Mammucari C., Milan G., Romanello V., Masiero E., Rudolf R., Del Piccolo P., Burden S. J., Di Lisi R., Sandri C., Zhao J., Goldberg A. L., Schiaffino S., Sandri M. (2007) FoxO3 controls autophagy in skeletal muscle in vivo. *Cell Metab.* 6, 458–471 [PubMed: 18054315]

54. Judge S. M., Wu C. L., Beharry A. W., Roberts B. M., Ferreira L. F., Kandarian S. C., Judge A. R. (2014) Genome-wide identification of FoxO-dependent gene networks in skeletal muscle during C26 cancer cachexia. *BMC Cancer* 14, 997 [PMCID: PMC4391468] [PubMed: 25539728]

55. Piao L., Sidhu V. K., Fang Y. H., Ryan J. J., Parikh K. S., Hong Z., Toth P. T., Morrow E., Kutty S., Lopaschuk G. D., Archer S. L. (2013) FOXO1-mediated upregulation of pyruvate dehydrogenase kinase-4 (PDK4) decreases glucose oxidation and impairs right ventricular function in pulmonary hypertension: therapeutic benefits of dichloroacetate. *J. Mol. Med. (Berl.)* 91, 333–346 [PMCID: PMC3584201] [PubMed: 23247844]

56. Araki M., Nakagawa Y., Oishi A., Han S. I., Wang Y., Kumagai K., Ohno H., Mizunoe Y., Iwasaki H., Sekiya M., Matsuzaka T., Shimano H. (2018) The peroxisome proliferator-activated receptor α (PPARα) agonist pemafibrate protects against diet-induced obesity in mice. *Int. J. Mol. Sci.* 19, pii: E2148 [PMCID: PMC6073532] [PubMed: 30041488]

57. Sugden M. C., Bulmer K., Holness M. J. (2001) Fuel-sensing mechanisms integrating lipid and carbohydrate utilization. *Biochem. Soc. Trans.* 29, 272–278 [PubMed: 11356166]

58. Degenhardt T., Saramäki A., Malinen M., Rieck M., Väisänen S., Huotari A., Herzig K. H., Müller R., Carlberg C. (2007) Three members of the human pyruvate dehydrogenase kinase gene family are direct targets of the peroxisome proliferator-activated receptor beta/delta. *J. Mol. Biol.* 372, 341–355 [PubMed: 17669420]

59. Shrivastav S., Zhang L., Okamoto K., Lee H., Lagranha C., Abe Y., Balasubramanyam A., Lopaschuk G. D., Kino T., Kopp J. B. (2013) HIV-1 Vpr enhances PPARβ/δ-mediated transcription, increases PDK4 expression, and reduces PDC activity. *Mol. Endocrinol.* 27, 1564–1576 [PMCID: PMC3753422] [PubMed: 23842279]

60. Fukawa T., Yan-Jiang B. C., Min-Wen J. C., Jun-Hao E. T., Huang D., Qian C. N., Ong P., Li Z., Chen S., Mak S. Y., Lim W. J., Kanayama H. O., Mohan R. E., Wang R. R., Lai J. H., Chua C., Ong H. S., Tan K. K., Ho Y. S., Tan I. B., Teh B. T., Shyh-Chang N. (2016) Excessive fatty acid oxidation induces muscle atrophy in cancer cachexia. *Nat. Med.* 22, 666–671 [PubMed: 27135739]

61. Koves T. R., Ussher J. R., Noland R. C., Slentz D., Mosedale M., Ilkayeva O., Bain J., Stevens R., Dyck J. R., Newgard C. B., Lopaschuk G. D., Muoio D. M. (2008) Mitochondrial overload and incomplete fatty acid oxidation contribute to skeletal muscle insulin resistance. *Cell Metab.* 7, 45–56 [PubMed:

18177724]

62. Warburg O. (1956) On the origin of cancer cells. *Science* 123, 309–314 [PubMed: 13298683]

63. Dang C. V. (2012) Links between metabolism and cancer. *Genes Dev.* 26, 877–890 [PMCID: PMC3347786] [PubMed: 22549953]

64. Leclerc D., Pham D. N., Lévesque N., Truongcao M., Foulkes W. D., Sapienza C., Rozen R. (2017) Oncogenic role of PDK4 in human colon cancer cells. *Br. J. Cancer* 116, 930–936 [PMCID: PMC5379150] [PubMed: 28208156]

Figures and Tables

Figure 1

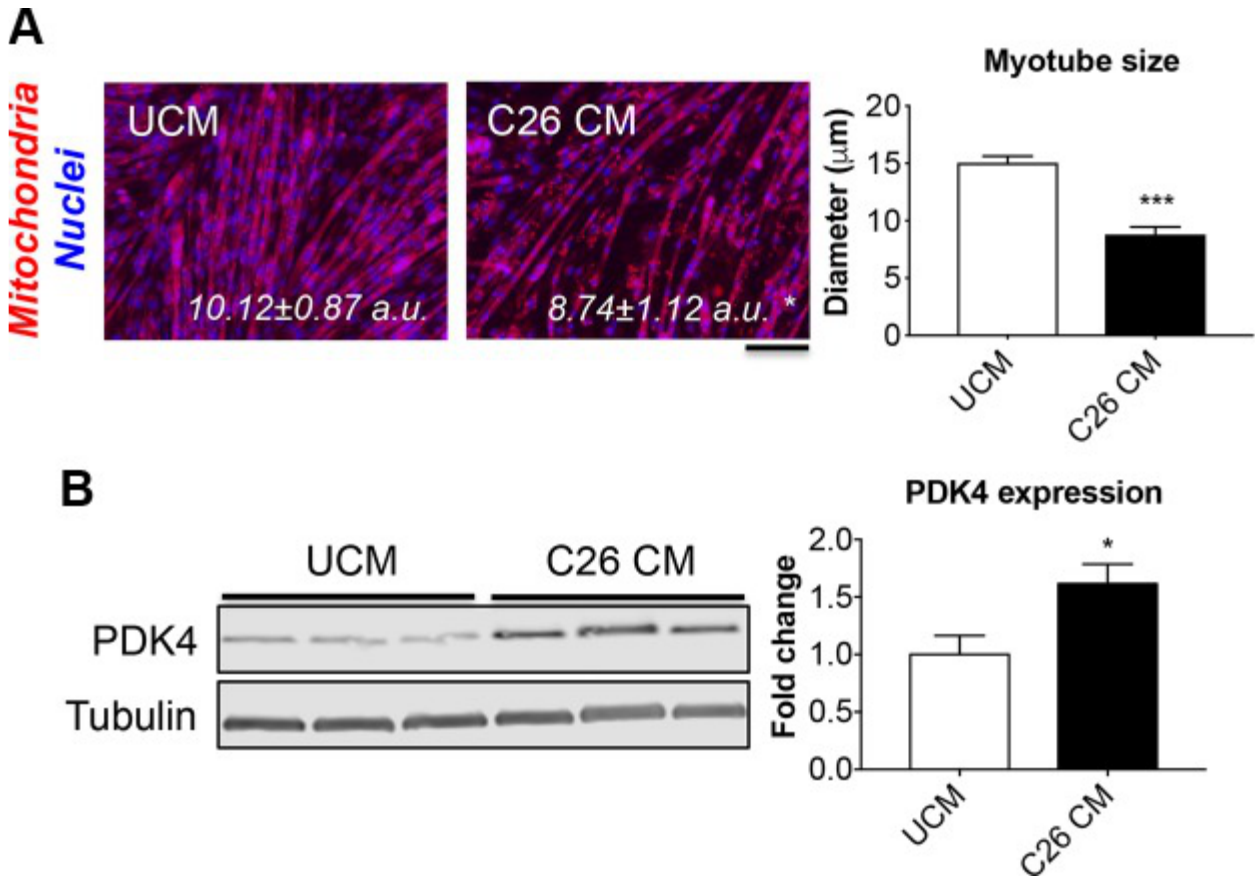

PDK4 is elevated in an *in vitro* model of cancer-induced atrophy. *A*) Representative images of C2C12 myotubes exposed to control medium (25% UCM) or 25% C26 CM for up to 48 h. The cell layers were stained for MitoTracker Red CMXRos, and the quantification of red fluorescence intensity (polarized mitochondria), normalized *vs.* DAPI (nuclei) was expressed as arbitrary units (a.u.). Myotube size was determined by measuring the minimum diameter of 250–350 myotubes per experimental condition (n = 3). Scale bar, 100 μm. *B*) Representative Western blotting for PDK4 in whole-protein extracts from C2C12

myotubes exposed to C26 CM (n = 3). Tubulin was used as loading control. Data (means ± SD) are expressed as fold change *vs.* UCM. *P < 0.05, ***P < 0.001.

Figure 2

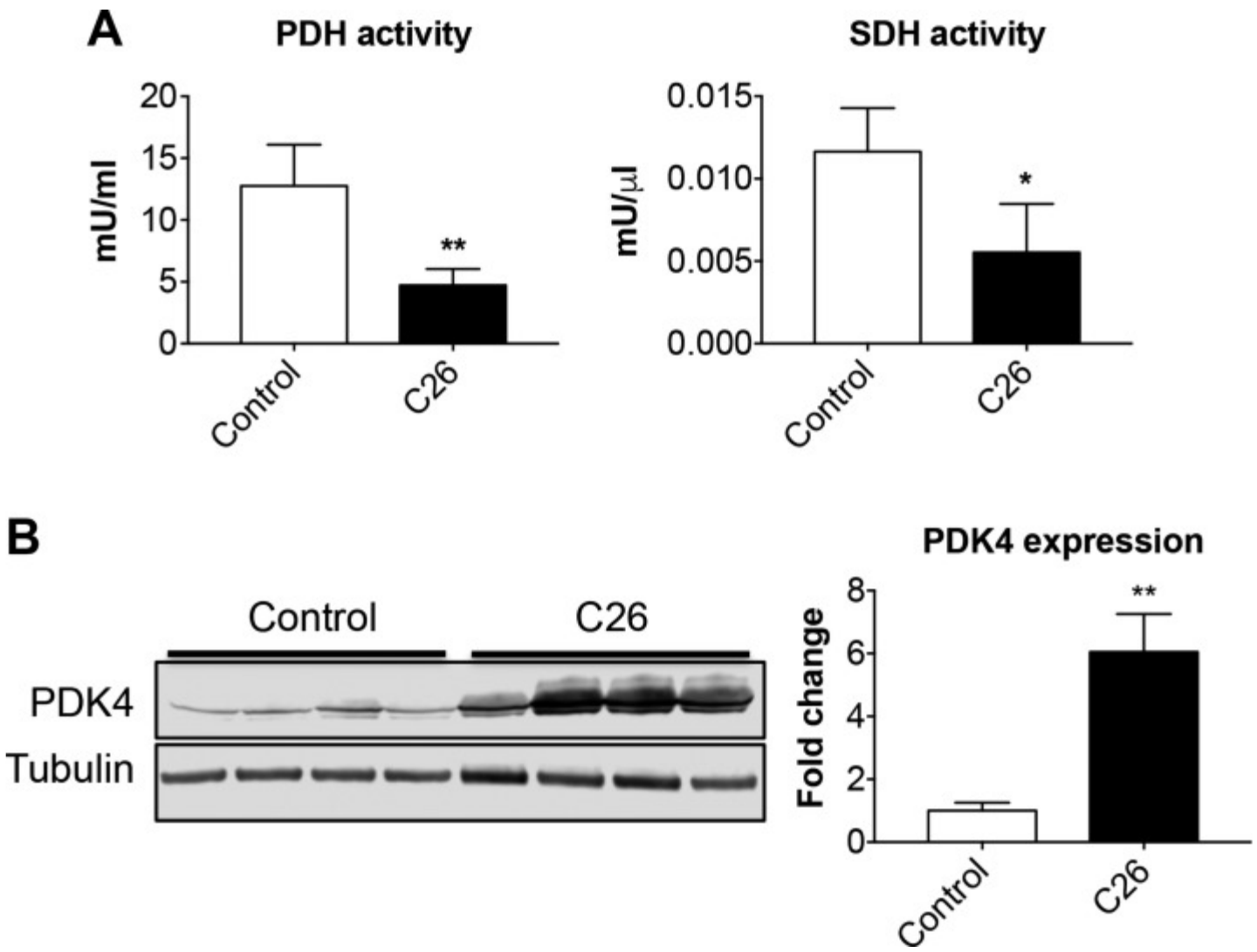

The C26 tumors cause significant metabolic derangements. *A*) Assessment of PDH and SDH enzymatic activities in gastrocnemius muscle of control and C26 tumor–bearing mice (C26). Data are expressed as mU/ml for PDH or mU/µl for SDH. *B*) Representative Western blotting for PDK4 in whole-muscle protein extracts from mice bearing the C26 tumor (n = 8). Tubulin was used as loading control. Data (means ± SD) are expressed as fold change *vs.* control. *P < 0.05, **P < 0.01.

Figure 3

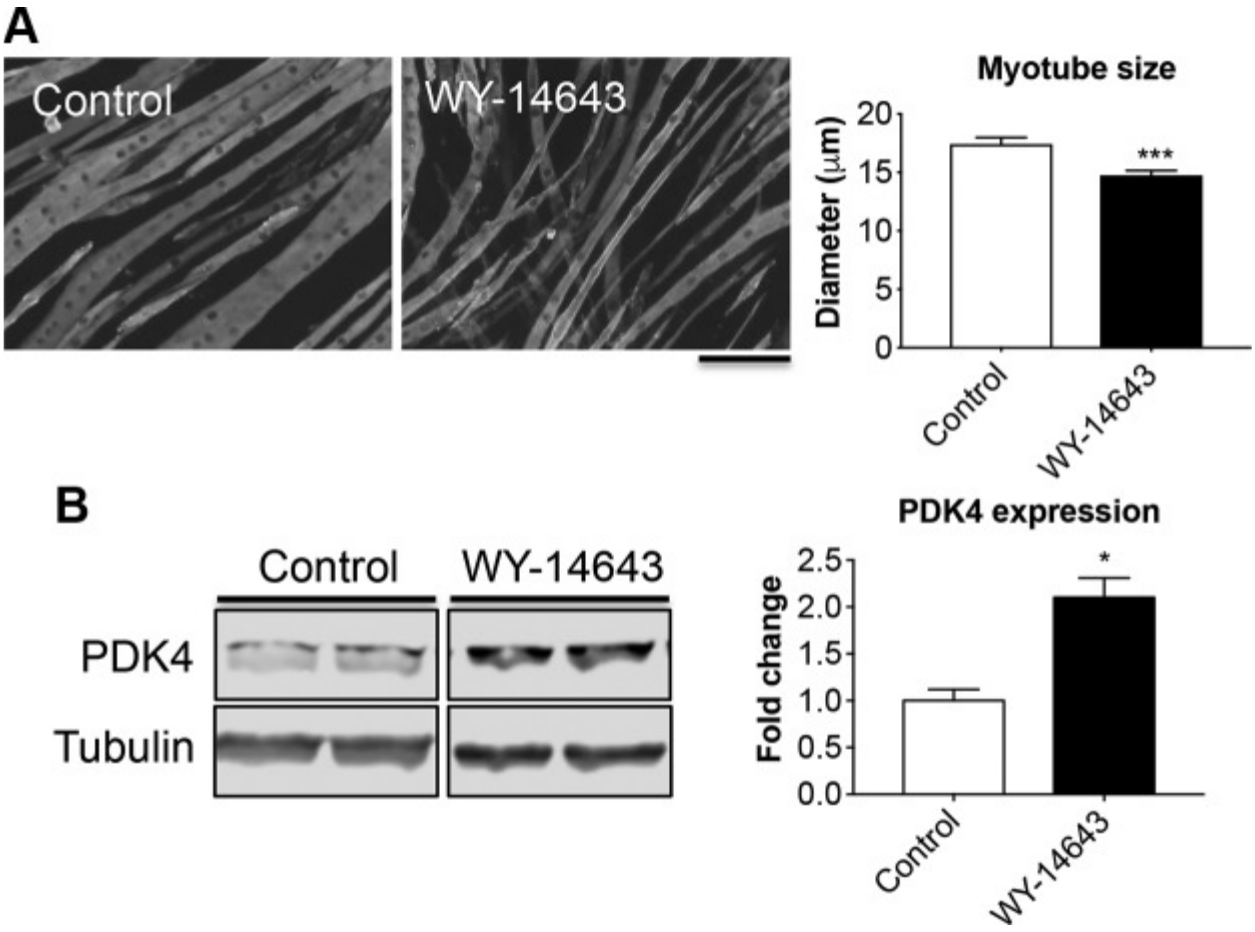

The PDK4 activator WY-14643 determines myotube atrophy. *A*) Assessment of myotube size in C2C12 cultures treated with WY-14643 for up to 48 h. On average, 250–350 myotubes were measured per experimental condition in triplicate. Green staining: myosin heavy chain. Scale bar, 100 μm. *B*) Representative Western blotting for PDK4 in whole protein extracts from C2C12 treated with WY-14643 ($n = 3$). Tubulin was used as loading control. Data (means ± SD) are expressed as fold change *vs.* control. $^{*}P < 0.05$, $^{***}P < 0.001$.

Figure 4

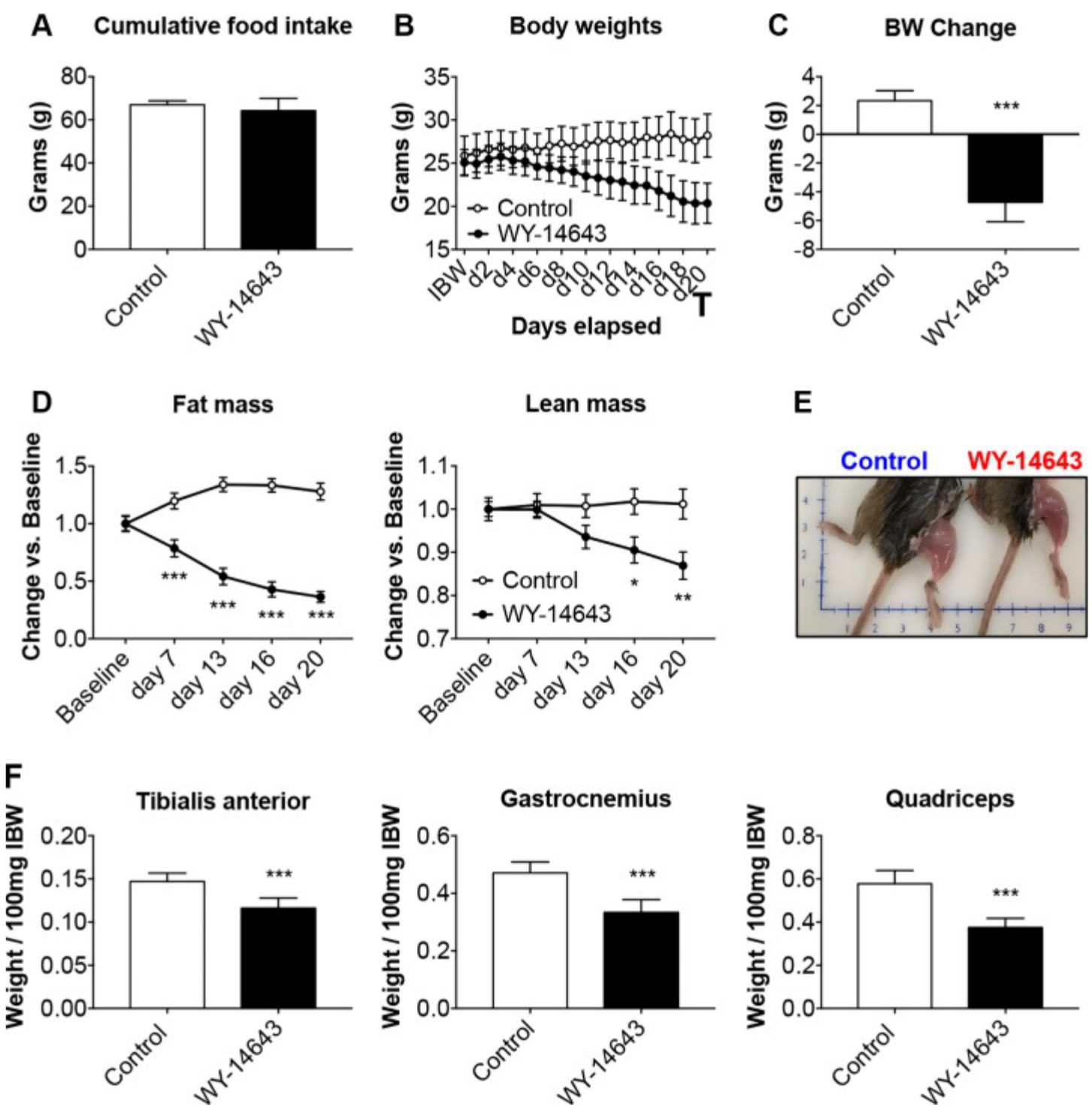

In vivo WY-14643 administration induces a cachectic phenotype. *A*–*C*) Cumulative food intake (*A*), body weight curves (*B*) and body weight change (*i.e.*, body weight at time of euthanization *vs.* initial body weight) (*C*) in mice fed a diet enriched with 0.1% WY-14643. *D*) Body composition assessment in mice fed WY-14643 was performed by means of EchoMRI. Data are expressed in grams of fat or lean tissue at time of euthanization. *E*) Representative image of hindlimb musculature in mice fed a control or WY-14643–enriched diet. *F*) Skeletal muscle weights (tibialis anterior, gastrocnemius, and quadriceps) in mice fed control or WY-14643 diets. Weights were normalized to the initial body weight (IBW) and expressed as weight/100 mg IBW; $n = 8$. Data are means ± SD. *$P < 0.05$, **$P < 0.01$, ***$P < 0.001$ *vs.* control.

Figure 5

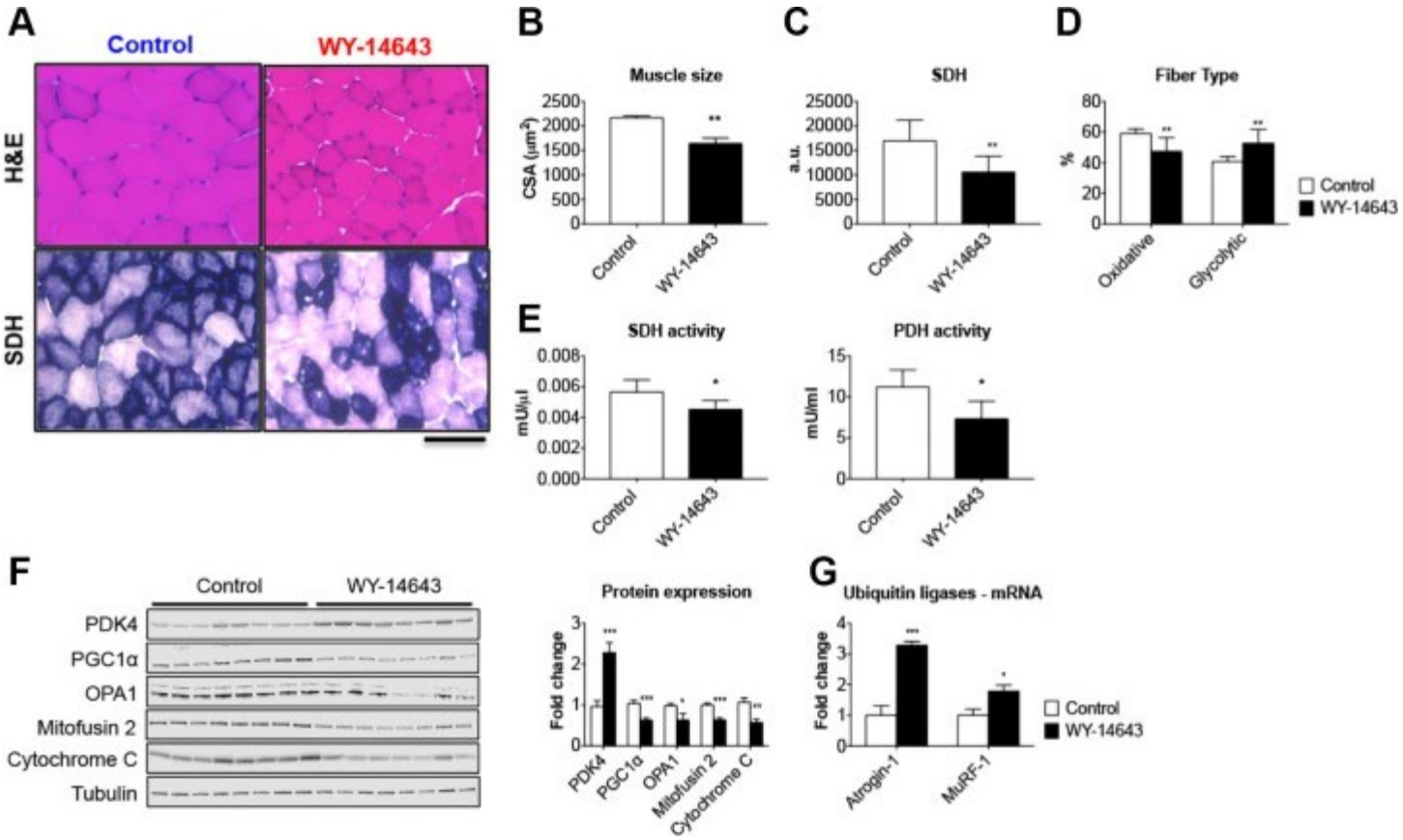

WY-14643 administration causes muscle atrophy and mitochondrial alterations. *A*) Representative images of hematoxylin and eosin (H&E)– and SDH-stained 10 μm-thick sections of tibialis anterior muscle excised from control and WY-14643–treated mice. Scale bar, 100 μm. *B*) CSA in tibialis anterior muscle sections from mice fed a diet enriched with WY-14643. *C*) Quantification of SDH integrated density in control and WY-14643–treated mice. Data are expressed as arbitrary units (a.u.). *D*) Number of oxidative (dark blue) and glycolytic (light blue) fibers (expressed as percentage of control). *E*) SDH and PDH enzymatic activities in the gastrocnemius muscle of control and WY-14643–treated animals. Data are expressed as mU/μl for SDH or mU/ml for PDH. *F*) Representative Western blotting for PDK4, PGC1α, OPA1, Mitofusin 2, and cytochrome *c* in whole-muscle protein extracts from mice fed control or WY-14643 diets. Tubulin was used as loading control. *G*) Gene expression levels for atrogin-1 and MuRF1 ubiquitin ligases performed by real-time quantitative PCR. Gene expression was normalized to TATA-binding protein levels. Data (means ± SD) are expressed as fold change *vs.* control; $n = 8$. *$P < 0.05$, **$P < 0.01$, ***$P < 0.001$.

Figure 6

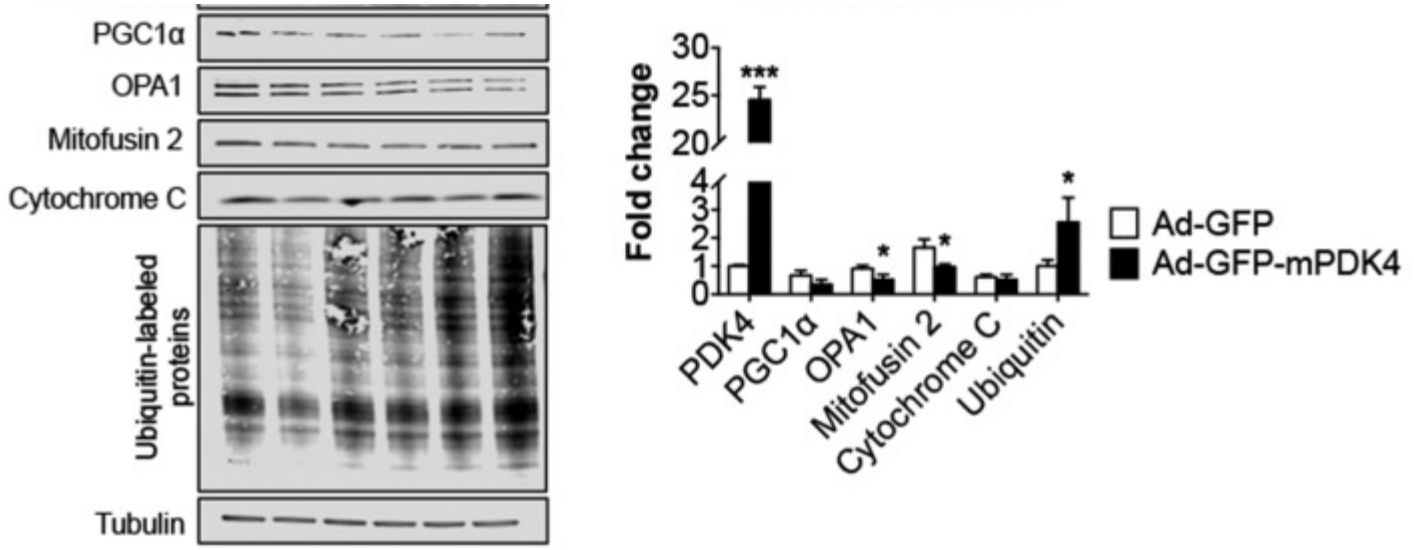
PGC1α
OPA1
Mitofusin 2
Cytochrome C
Ubiquitin-labeled proteins
Tubulin
Fold change
Ad-GFP
Ad-GFP-mPDK4
PDK4
PGC1α
OPA1
Mitofusin 2
Cytochrome C
Ubiquitin

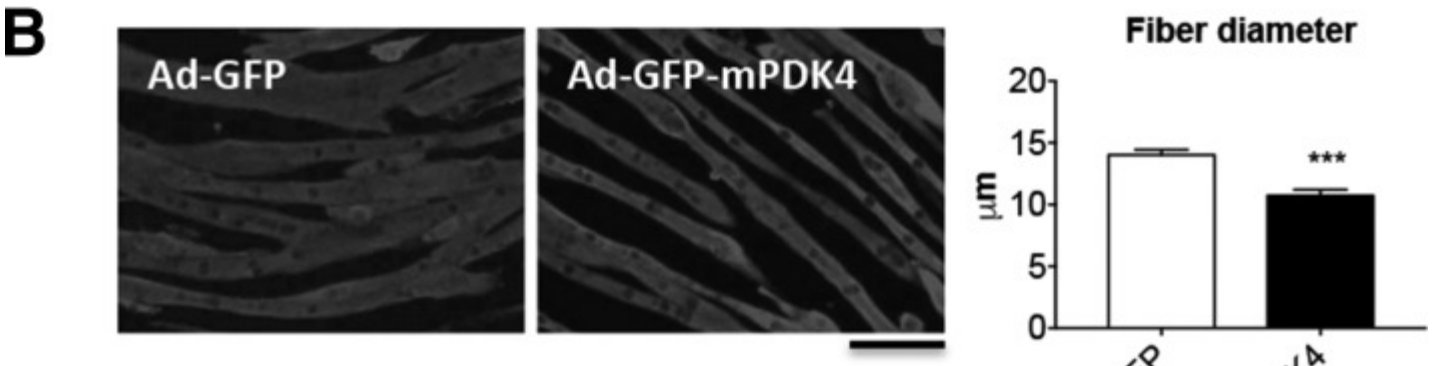
B
Ad-GFP
Ad-GFP-mPDK4
Fiber diameter
μm
Ad-GFP
Ad-GFP-mPDK4

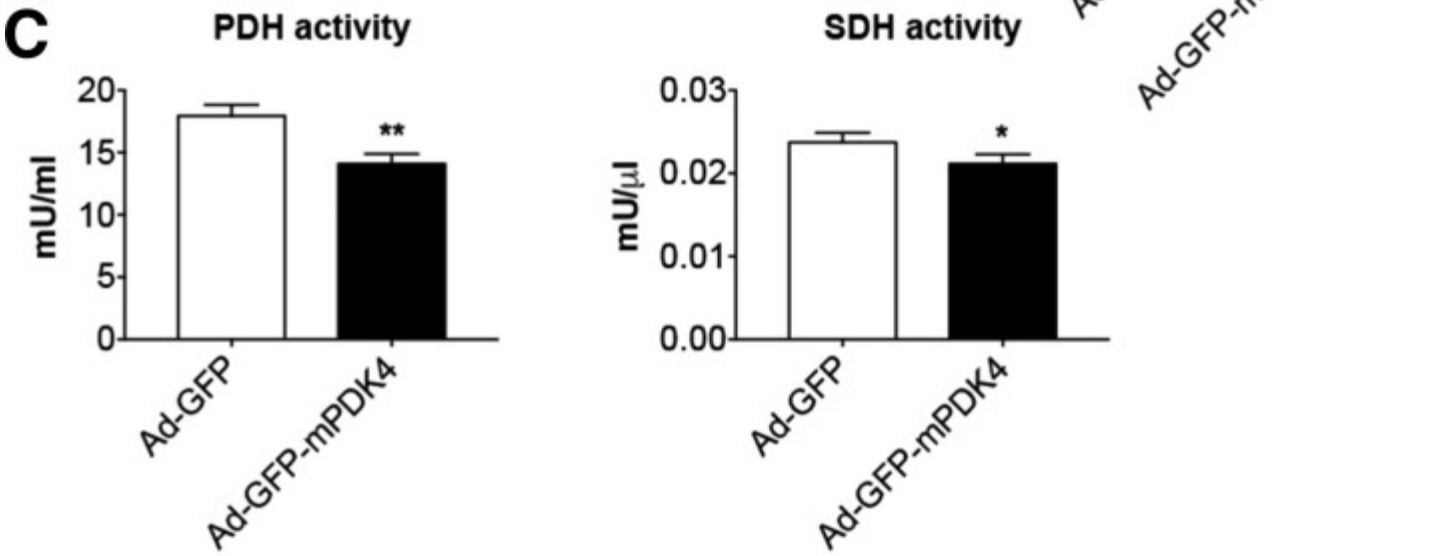
C
PDH activity
mU/ml
SDH activity
mU/μl
Ad-GFP
Ad-GFP-mPDK4

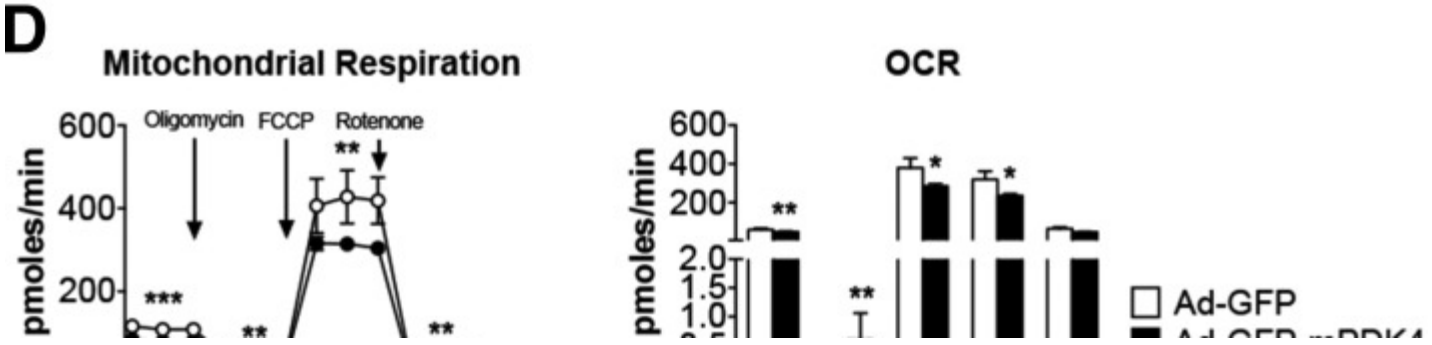
D
Mitochondrial Respiration
pmoles/min
Oligomycin
FCCP
Rotenone
OCR
Ad-GFP

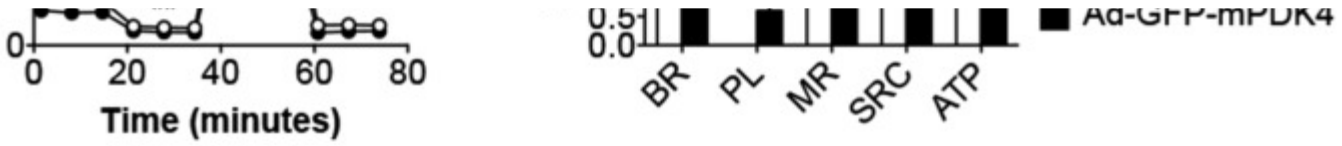

PDK4 overexpression affects C2C12 myotube size and metabolism. *A*) Representative Western blotting and quantification for PDK4 (shown with both low and high exposure times), PGC1α, OPA1, Mitofusin 2, cytochrome *c*, and ubiquitin-labeled proteins in C2C12 myotubes infected with Ad-GFP or Ad-GFP-mPDK4 ($n = 3$). Tubulin was used as loading control. *B*) Myosin heavy chain (MyHC) immunofluorescent staining in C2C12 myotubes infected with Ad-GFP or Ad-GFP-mPDK4 ($n = 3$) and myotube size quantification. On average, 250–350 myotubes were measured per experimental condition, in triplicate. Scale bar, 100 μm. *C*) Pyruvate dehydrogenase (PDH) and succinate dehydrogenase (SDH) enzymatic activities in C2C12 myotubes infected with Ad-GFP and Ad-GFP-mPDK4. Data are expressed as milliunits per millilter for PDH, or milliunits per microliter for SDH. *D*) Mitochondrial respiration and oxygen consumption rate (OCR) in C2C12 myotubes infected with Ad-GFP or Ad-mPDK4 ($n = 3$). ATP, adenosine triphosphate; BR, basal respiration; MR, maximal respiration; PL, proton leak; SRC, spare respiratory capacity. Data (means ± SD) were expressed in picomoles per minute. Data (means ± SD) are reported as fold change *vs*. Ad-GFP. $^{*}P < 0.05$, $^{**}P < 0.01$, $^{***}P < 0.001$ *vs*. Ad-GFP (significance of the differences).

Figure 7

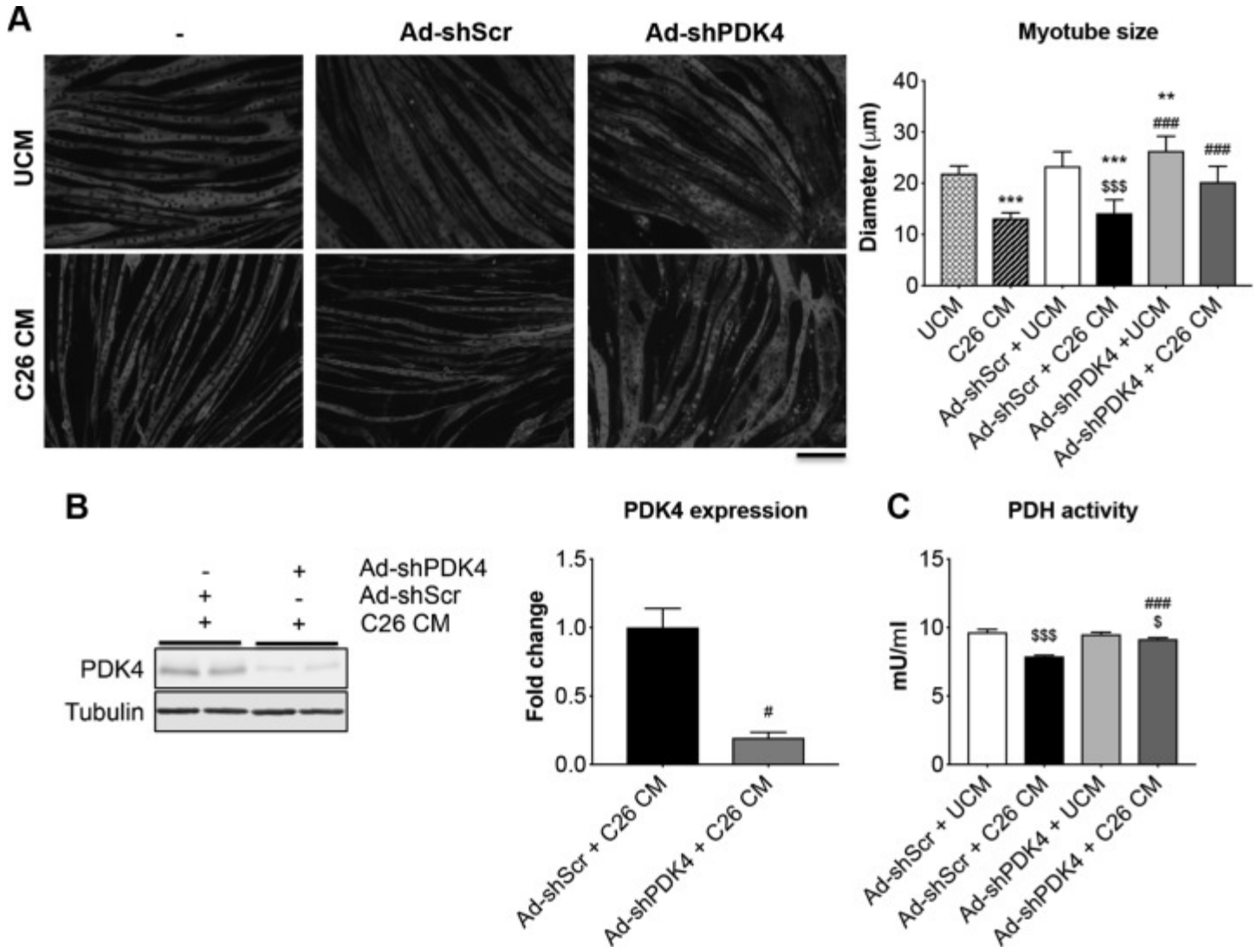

PDK4 deletion protects C2C12 myotubes from tumor-induced atrophy. *A*) Representative images of myosin heavy chain–stained C2C12 myotubes infected with either Ad-shScr or Ad-shPDK4 alone or in combination with either 25% control medium (25% UCM) or 25% C26 CM for up to 48 h. Data (means ± SD) are expressed as micrometers. On average, 250–350 myotubes were measured per experimental condition in triplicate. Scale bar, 100 μm. *B*) Representative Western blotting for PDK4 in whole protein extracts from C2C12 myotubes infected with Ad-shScr or Ad-shPDK4 and exposed to C26 CM for up to 48 h. Tubulin was used as loading control. *C*) PDH enzymatic activity in C2C12 myotubes infected with Ad-shScr or Ad-shPDK4 and exposed to C26 CM for up to 48 h. Data (means ± SD) are expressed as mU/ml. $^{**}P < 0.01$, $^{***}P < 0.001$ *vs.* UCM, $^{\$}P < 0.05$, $^{\$\$\$}P < 0.001$ *vs.* Ad-shScr + UCM, $^{\#}P < 0.05$, $^{\#\#\#}P < 0.001$ *vs.* Ad-shScr + C26 CM.